

tion (experimental accuracy 30%) has been made by M. Chen, LRL Report No. UCRL-18653, 1969 (unpublished).

⁴³W. Slater, D. H. Stork, H. K. Ticho, W. Lee, W. Chinowsky, G. Goldhaber, S. Goldhaber, and T. O'Halloran,

Phys. Rev. Letters 7, 517 (1961).

⁴⁴This follows by a straightforward calculation from the matrix element given by J. D. Jackson, *Elementary Particle Physics and Field Theory* [1962 Brandeis Summer Institute] (Benjamin, New York, 1963), p. 290.

PHYSICAL REVIEW D

VOLUME 4, NUMBER 1

1 JULY 1971

Muons Produced By Atmospheric Neutrinos: Experiment*

F. Reines, W. R. Kropp, H. W. Sobel, H. S. Gurr, and J. Lathrop
University of California, Irvine, California 92664

and

M. F. Crouch

Case Western Reserve University, Cleveland, Ohio 44106

and

J. P. F. Sellschop and B. S. Meyer†

University of the Witwatersrand, Johannesburg, Republic of South Africa
(Received 8 February 1971)

The interaction of high-energy muon neutrinos produced in the atmosphere by primary cosmic rays has been observed deep underground (8.74×10^5 g cm⁻² std. rock) in the rock surrounding a large-area (160 m²) liquid-scintillation-detector hodoscope. A series of arguments is given to separate the residual atmospheric muons which reached the detector from those produced by neutrino interactions in the surrounding rock. These arguments are based on the widely differing angular distributions and mean energies of the two sources. The observation of four events arising from the decay of muons stopping in the detector suggests that the energy of neutrino-induced muons is $\sim \frac{1}{2}$ GeV. Operation of the system over a three-year period yielded a total of 39 which we identify as neutrino-produced muons. Of these, 35 were in the aperture chosen for the observation of neutrino-induced muons, yielding a total rate of $(6.5 \pm 1.1) \times 10^{-7}$ sec⁻¹. In a companion paper, this result is compared with rates predicted using various theoretical models of the neutrino-nucleon interaction. This comparison selects the most appropriate model and leads to an underground neutrino-induced muon flux. In the present paper the simplifying approximation of an isotropic neutrino distribution leads directly to a flux of $(3.7 \pm 0.6) \times 10^{-13}$ cm⁻² sec⁻¹ sr⁻¹.

I. INTRODUCTION

High-energy neutrinos resulting from the interaction of primary cosmic rays with the earth's atmosphere have long been considered a possible tool for the investigation of the weak interaction.¹⁻³ Interest in such experiments was heightened with the discovery of the accelerator-produced, muon-associated neutrino in 1962.⁴ In undertaking the present experiment, it was anticipated that the higher-energy neutrinos available in the secondary cosmic rays might cast light on the question of the existence of a mediating vector boson for the weak interaction as well as reveal something of the character of the interaction cross section for neutrinos with energies in excess of those available at accelerators. In addition to these definable goals was the hope that a more sensitive search for cosmic-

ray neutrinos might yield information as to hitherto unsuspected sources or interactions.

Assuming a cross section in the vicinity of 10^{-38} cm²/nucleon, and calculations of the atmospheric neutrino spectrum and flux based on measurements of atmospheric muons produced in the decay processes associated with these neutrinos, it was estimated by various authors¹⁻³ that a detector of effective mass measuring a few thousand tons would be required to yield a signal of several events per year. Since the neutrino interaction was signaled by a muon, it was immediately evident that, unless special steps were taken, such a large detector would be flooded with a background arising from atmospheric muons which was some 10^{10} times as intense as the expected signal. Two variants to reduce the background below that expected at sea level were the use of a moderate depth in conjunc-

tion with the requirement that the muon produced in the neutrino interaction be travelling upward, or the use of a simpler detector located at such a great depth that the atmospheric muon flux would be reduced to negligible proportions. A conservative approach, employing an ultradeep location was adopted when it was learned⁵ that the cosmic-ray muon intensity is acceptably low at the two-mile depths which could be made available in a South African gold mine.

The great range of the product muon was a key feature in the economical design of the detector as this enabled the use of a large-area detector to observe neutrino interactions occurring in a great mass of surrounding rock.

A laboratory was prepared and a large-area scintillation detector developed, installed, and operated.⁶ The present paper discusses the experimental details and concludes with a rate for observing neutrino-induced muons. A companion paper⁷ presents the theoretical analysis.

II. DESCRIPTION OF EXPERIMENTAL SITE AND EQUIPMENT

A. The Site

The experiment was located at a depth of $8.71 \times 10^5 \text{ g cm}^{-2}$ below the surface in the Hercules shaft of the East Rand Proprietary Mine (ERPM) near Johannesburg.⁸ The experimental site was divided into two areas, the control chamber and the detector tunnel. The control chamber, in which were located a house containing the major portion of the electronics, the house air conditioning plants, and the motor-generator unit, was a room 2.6 m by 6 m in cross section and 9 m in length. The detector tunnel was 3 m by 3 m in cross section and 150 m in length, following an approximate north-south line. Access to the site was provided by a vertical shaft followed by three inclined shafts.

At these great depths, the virgin rock temperatures are in the vicinity of 123°F , necessitating air conditioning of the entire site. While additional air conditioning was required for the electronics

house, standard mine ventilation maintained adequately low tunnel temperature ($\sim 85^\circ\text{F}$) and relative humidity ($\sim 75\%$). The thermally insulated house was maintained at an average temperature of $\sim 75^\circ\text{F}$ and a relative humidity $\leq 45\%$.

Electrical power was supplied through a motor generator to isolate the site from electrical noise on the mine power line. High frequencies present on the generator output were reduced by isolating transformers and LC filters. External high-frequency noise was further reduced by covering the electronics house with close-mesh wire screening.

B. The Detector

The detector array, shown schematically in Fig. 1, consisted of 54 liquid-scintillation-detector elements, arranged in two discontinuous rails, one on the east side of the tunnel and one on the west side, having a total area of about 160 m^2 . Each element was an ultraviolet-transmitting Lucite tank filled with liquid scintillator and viewed from each end by two 5-in. photomultiplier tubes. The tubes on one end were labeled A, B, and those on

TABLE I. Dimensions of the detector elements and their spacing in the array. Directions are defined in Fig. 1.

	Bays 1-6 (m)	Bays 7-9 (m)
Length	5.47	4.71
North-south gap	0.59	1.36
Thickness	0.127	0.127
East-west gap	1.65	1.70
Height	0.555	0.555
Vertical gap	0.150	0.171

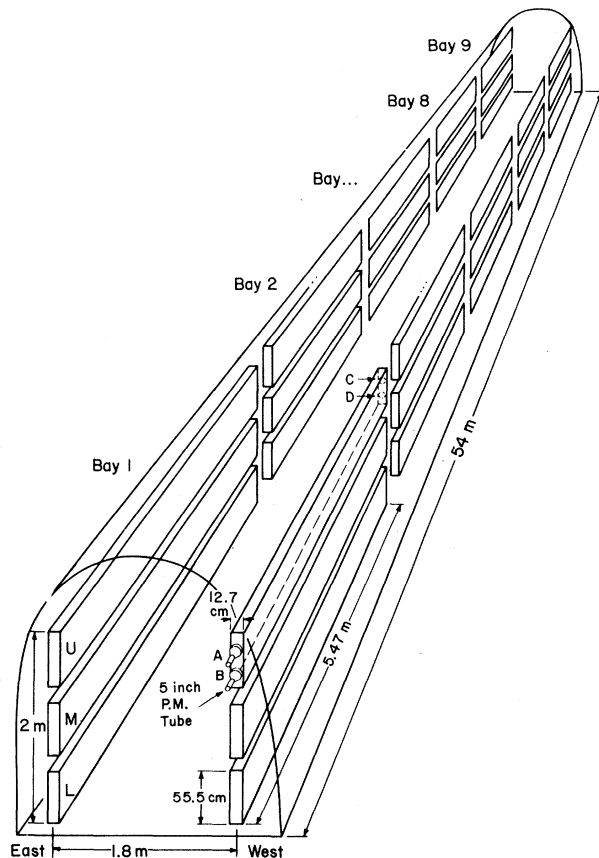


FIG. 1. Sketch of the detector array. Approximate array and element dimensions are given.

the other C, D. The dimensions and spacings of the elements in the array are given in Table I.

The design of the detector elements was dictated by the need for

- (1) a large and relatively inexpensive surface area viewed by a small number of photomultiplier tubes,
- (2) a thickness sufficient to ensure energy deposition by a penetrating charged particle well in excess of that due to natural radioactivity,
- (3) a height consistent with the tunnel dimensions and the desired hodoscope angular resolution,
- (4) a response function such that pulse height variations over the length of the element were not excessive.

The CERN technique⁹ using plastic containers with totally reflecting walls was found to enable construction of detectors of quite substantial size having remarkably good characteristics.¹⁰ The Lucite tanks were housed in a close-fitting box with white-painted inside surfaces to serve as a light-tight housing and backup reflector.

1. Detector Response Function: Position of Scintillation Event and Energy Deposition

The energy deposited in the detector by a muon varied, depending on the length of path in the scintillator, on Landau fluctuations and, to a lesser extent, on the muon energy which in most cases was in the GeV range. A horizontally moving muon deposited ~ 20 MeV, while one moving vertically deposited ~ 90 MeV. The fraction of the scintillation light reaching the photomultiplier tubes depended on the location of the scintillation within the element. The detector response was studied with identical elements at the surface of the earth, selecting atmospheric muons with known paths by means of two small guide detectors. The response function, i.e., the relative signal amplitude seen by a photomultiplier as a function of event location is shown in Fig. 2, as is the derived ratio of the average signal from the pair of photomultipliers at one end of the element to the average signal from the pair at the other end. The ratio of pulse heights gave the center position of the scintillation along the active length of the element to within ± 0.15 m, irrespective of the path length in the scintillator.

The response function in conjunction with an energy calibration determines the energy deposited in the detector. The error in estimating path length, or equivalently (in the approximate sense outlined above) the error in the energy deposited in the scintillator, is found to be roughly constant (± 16 MeV), independently of orientation and location in the element, e.g., within $\pm 50\%$ for nearly horizontal paths and within $\pm 20\%$ for vertical paths.

The above discussion applies only to events involving a single particle or multiple particles which are close together.

2. Background Effects of Natural Radioactivity

A number of modifications of the basic detector element design were necessitated by the rather high level of radioactivity in the detector tunnel. Most triggers of the recording system were due to the chance time coincidence within resolving time of the electronic circuitry (~ 0.8 μ sec), of a γ -ray absorption process near the A, B end of one detector and an unrelated γ process at the C, D end of the same (or another) detector. The steeply rising response function of the detector elements gave such a chance coincidence the appearance of a higher-energy single interaction. Thus as one lowered the energy threshold so as to see horizontally penetrating events (≥ 15 MeV) at the far end of the detector, the rate of system triggers became unacceptably high. There also existed the possibility of such chance γ rays interacting in the same element within the resolving time of the system, ~ 0.2 μ sec, as determined from inspection of the oscilloscope records, thereby simulating the signature of a single tank event. While such events would not be of high energy, they would be similar to those produced by corner-cutting cosmic rays. In addition, the chronotron data-recording system added the output signals from as many as 72 photomultiplier tubes and displayed them on a single oscilloscope trace. The result, which depended on the number of γ 's seen by each tube, was a general noise level which made timing and amplitude measurements of small signals difficult.

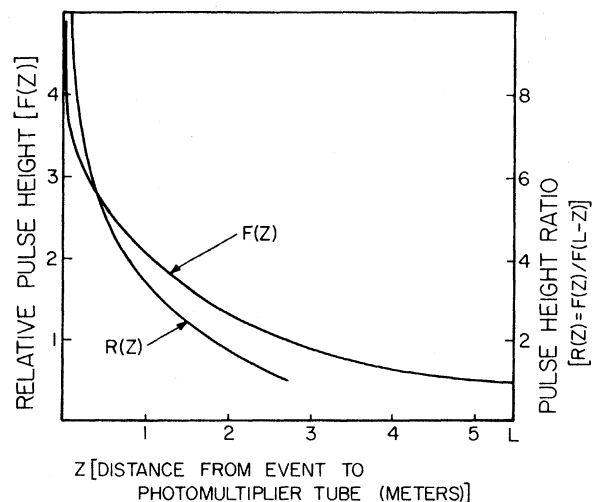


FIG. 2. The response function of an element from bays 1-6 and the dependence of the pulse height ratio on event position.

Several methods were used to combat these effects:

(1) Transparent vertical partitions were added to some elements 38 cm from each end. The end regions were then filled with nonscintillating mineral oil.

(2) Opaque horizontal partitions 38 cm in length were placed in the liquid at the ends of some elements to isolate optically the A from B photomultipliers and similarly the C from D photomultipliers.

(3) The white diffuse reflective coating was removed from the light tight housing in the end regions of those elements with horizontal partitions.

Method (1) was employed in bays 7 to 9, which were added to the original system (bays 1 to 6) after the background problem had been assessed. Methods (2) and (3) were employed in bays 1 to 6 where detector elements were of the original design.

The detailed effects of these measures are considered elsewhere.¹¹ In brief, they were successful in reducing the difficulties discussed above to an acceptable level.

C. The Detector Hodoscope

Referring again to Fig. 1, an address can be assigned to each element. Each group of six tanks (three in the east rail and three in the west rail) was referred to as a bay. Within each bay the designation of east or west and of upper, middle or lower determined a specific element. Thus, the address E5M refers to the middle tank in bay 5 on the east side.

In this manner, the detector array formed a hodoscope locating single-element events in two dimensions along the detector tunnel, and determining crude angular coordinates of the event trajectory¹² for two and three element events. The event positions determined the angle relative to the longitudinal axis of the array. In the plane perpendicular to this axis, three angular ranges could be distinguished on each side of the horizontal. These were $\sim 0-20^\circ$, $\sim 20-40^\circ$, and $\sim 40-50^\circ$. As noted below, this interpretation of the event was unambiguous except for those rare events which involved more than one bay on the same side of the array. The scintillation detector was, of course, unable to determine the direction of travel of the particle.

Two additional bays (10 and 11) were operated briefly. Each bay consisted of three standard scintillation elements (forming one side of a normal bay) and eight Čerenkov detectors. The object was to infer the direction of travel of any particles traversing the detectors. The Čerenkov detectors were similar in design to the scintillation tanks,

but only about half as long, filled with water, and viewed by two photomultipliers, one at each end. These detectors were positioned next to the scintillators, but were vertically oriented with one photomultiplier at the top, and one at the bottom. The relative sizes of the top and bottom phototube signals together with the location of the event in the detector determined, in principle, the direction of travel of the particle. The data obtained from these detectors was of limited utility, principally because of their small aperture and the crudeness of the position information supplied by the scintillation elements. Of the events recorded, most appeared to be downward going. One event, apparently upward going, was studied in detail. Based on the characteristics of the detectors, this direction assignment is about 90% certain.

D. Electronics

Two complete and separate data recording systems, the "chronotron" and the "charge storage," were developed for use with the detector hodoscope. Each met the problem of handling large numbers of photomultiplier signals (initially 144 and finally 216) in a different and complementary fashion. Subsequently, as knowledge of the character of the events under study was gained, it was possible to modify the chronotron so as to eliminate the need for the charge storage system.

1. The Charge Storage System

This system handled large numbers (144) of simultaneously occurring signals by storing them as charges on individual capacitors. Subsequently the charges were measured and their values digitized in sequence. The resulting numbers, which represented the original pulse amplitudes, were stored in serial fashion in the memory of a pulse-height analyzer. The main advantage of this system was that it recorded the output of each photomultiplier separately and thus unambiguously. The chief disadvantage was its inability to preserve signal-wave form, a feature which restricted the realizable coincidence resolving time and severely limited its ability to distinguish between bona fide and spurious signals. Details may be found in Ref. 13.

2. The Chronotron

In an experiment designed to detect events occurring as infrequently as ten per year, a visual record of the actual waveforms is of great value in identifying the signal. By considering the various kinds of events which might be observed with the array, it was possible to devise a relatively simple sys-

tem in which signals were combined to generate a pulse position code enabling nearly all physically interesting events to be displayed unambiguously, using only two dual-beam oscilloscopes. The system was called a "chronotron" because it preserved the time relationships between pulses.

Examples of events recorded with the chronotron as well as an explanation of the position code are given in Fig. 3.

Ambiguities in event location were a minor problem. In the final form of the chronotron, all types of events involving elements in a single bay were displayed in an unambiguous fashion. Uncertainties arose only when two (or more) upper or middle or lower elements on the same side of the array were involved. In these relatively rare cases (Table II), the elements could usually be identified, but only limits could be established for the energies and locations.

Details of the chronotron are found in the Appendix.

E. The Monitoring System

The individual components of the detector hodoscope were highly reliable, but their large number led to a finite, though small, failure rate. This multiplicity made it important to have a quick and easy method for testing the correct operation of the entire array. In addition, an automatic system was required to provide a record of the detailed behavior of the detector during the long periods – up to one week – of unattended operation. These ends were achieved by means of a light-pulsar array¹⁴ designed around small corona lamps installed in each element. When a single lamp was pulsed, it simulated the passage of an ionizing particle through its element, so triggering the electronic system. The visual or film record of the event demonstrated the operability of the associated electronics and gave crude information on calibration and stability. Individual lamps could be activated remotely either by the system operator or by an automatic sequencing device. This latter device operated periodically whenever the hodoscope was collecting data, providing checks of the entire system.

III. CALIBRATION

Calibration of large scintillation detectors is a major problem at great depths due to the paucity of atmospheric muons ordinarily used at shallow depths or on surface. Accordingly, we located a standard detector element on the surface of the earth, calibrated it using cosmic-ray muons, and related the muon signal to a portable secondary

standard for use underground.

In the early stages of the experiment an ^{88}Y γ -ray source (0.9 MeV and 1.8 MeV) was used as the secondary standard. The spectral response of the detector elements to the source showed no structure, so the integral count above some pulse height, or the matching of spectral shapes was used. This approach has several shortcomings related to the variation of the detector response with source position. Because of its low energy relative to that for which the detector elements were designed, the secondary source could only be seen when located very near to the photomultipliers. This provided a test involving the scintillation efficiency of the liquid, but not is optical transmission. In addition,

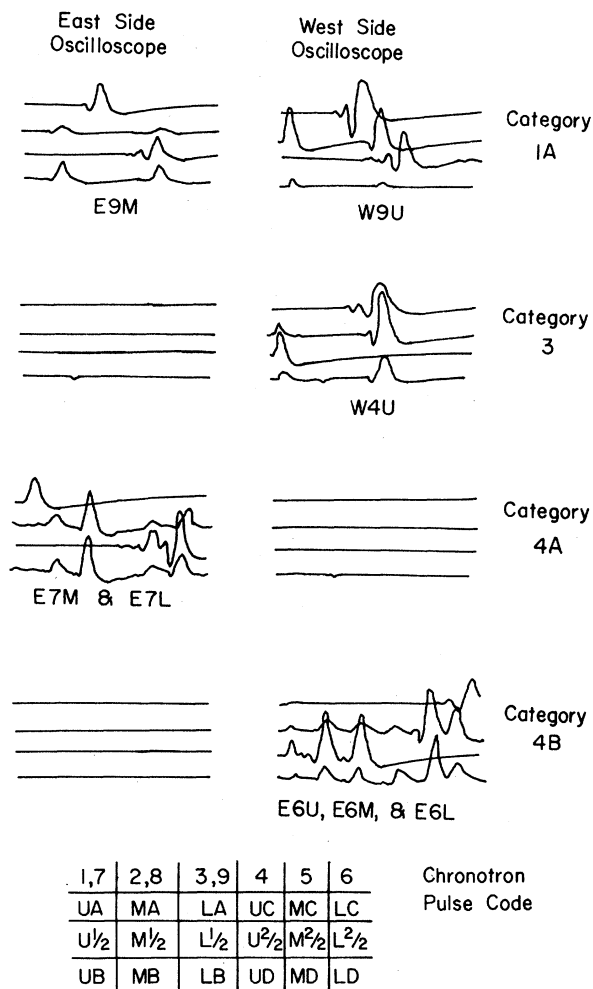


FIG. 3. Typical oscilloscope records of events involving categories 1A, 3, 4A, and 4B. The pulse code is also shown. The letters E (east) and W (west) designate the two sides of the array; U (upper), M (middle), and L (lower) the position on a given side and A, B, C, and D the four photomultiplier positions on each element. The numbers 1–9 specify the 9 bays while 1/2 and 2/2 refer to bays 1–6 and bays 7–9, respectively.

TABLE II. Definitions, populations, and sensitive times for the various data categories. Based on data collected between 30 October 1964 and 23 August 1967. Instrumental dead-time corrections have been made.

Category	Number of detector elements involved	Locations of signals in array	Bays 1-6		Bays 7-9	
			Observed population	Sensitive time (h)	Observed population	Sensitive time (h)
1A	2	1 east side, 1 west side	24	16 579	8	12 110
1B	3	2 on one side, 1 on the other	6	14 349	0	12 110
2A	>3	both sides	8	13 187	2	11 706
2B	≥ 2	not classifiable into other categories	1	14 671	0	12 022
3	1	anywhere in array	143	13 075	69	11 229
4A	2	adjacent elements, one above the other	37	14 671	14	11 562
4B	3	adjacent elements, one above the other	25	14 671	5	11 562
5	1	two signals a few microseconds apart	4	16 579	0	12 110

it was found that the presence of cosmic-ray background in the surface detector introduced large uncertainties in the response to the ^{89}Y source and, hence, in relating the primary and secondary standards. Finally, this source was of little value in calibrating the modified detectors of bays 7 to 9 due to the presence of the inert regions.

The above difficulties ultimately led to the use of a pulsed light source¹⁴ as the secondary standard. The need for a system whose gain could be kept constant over long periods of time and varying environmental conditions was met by introducing an additional step in the calibration procedure: the cross referencing of the light source to a radioactive source by means of a portable scintillation detector.

A third method, employing the ^{89}Y source and reflective baffle which optically isolated a small volume of scintillator adjacent to a single photomultiplier was found useful on occasion. This geometric arrangement produced a spectrum with structure which could be related to the surface muon calibration. This technique was used mainly as a check of the previously described methods since its employment involved disassembly of the detector elements and was inordinately time consuming.

These techniques resulted in an absolute energy calibration with a precision of $\pm 10\%$. Monthly system calibrations maintained the over-all gain within this range for the duration of the experiment.

Various energy thresholds ranging from 5 to 9 MeV for events occurring at the center of a detector element, were employed. The response function (Fig. 2) determined the threshold at other locations. For example, 5 MeV center of tank

implied a threshold of only ~ 0.8 MeV for an energy deposition in the immediate vicinity of a photomultiplier. This was the source of most of the difficulties produced by natural radioactivity, and the reason for the detector modifications described earlier. The thresholds chosen were determined by the desire to see penetrating events at the far end of the detector and by a consideration of the acceptable trigger rate. It is to be noted that, because of the nonlinear spatial response of the detectors, the energy threshold determines the efficiency of the array for detecting penetrating particles.

IV. BACKGROUNDS

A. Natural Sources

Natural sources other than cosmic rays can be dismissed on the basis of energy considerations: The minimum energy deposited in the detector in an acceptable neutrino event was 24 MeV while the average deposition was in excess of 40 MeV (Table III).

B. Artificial Sources

The low rate of events due to all cosmic rays, about one in two days, required special precautions to ensure that the system discriminated against electrical noise and other instrumental effects.¹⁵ One such background, that associated with seismic disturbances, is unique in our deep underground location.

Early in the operation of the detector, it was observed that violent earth movements were capable of producing signals which satisfied the electronic

TABLE III. A listing of the category 1A and 1B events which have been attributed to neutrinos and used in our calculation. Included is the time, location in array, energy deposition, and sidereal coordinates.

Date	G.M.T.	Elements	Energy deposition (MeV)	Right ascension (deg)	Declination (deg)
23 Feb. 1965	20:47	E4L	29	219.9±12.9	7.3±7.9
		W4L	18		
28 Feb.	23:20	E5M	55	119.1±11.9	13.3±9.7
		W5U	118		
17 Mar.	17:52	E4L	19	58.9±11.5	50.9±9.5
		W4L	16		
20 Apr.	13:15	E2M	24	13.1±13.0	43.2±10.1
		W2M	24		
1 June	21:36	E1L	22	326.6±12.6	11.6±7.3
		W2L	19		
3 June	00:41	E4U	8	176.8±11.8	8.0±8.2
		W4M	26		
1 July	14:19	E3M	19	255.2±11.4	27.7±5.5
		W3U	26		
21 Nov.	14:06	E4L	Large
		W4L	25		
7 Dec.	16:42	E3U	38	271.8±14.0	13.6±9.9
		W3U	23		
25 Dec.	06:15	E5L	20	142.1±13.9	30.0±10.5
		W5L	20		
30 Dec.	00:47	E9M	22	129.3±2.7	54.2±5.8
		W9U	14		
28 Feb. 1966	03:04	E8U	19	155.0±14.1	24.8±10.4
		W8U	17		
1 Apr.	07:20	E9U	8	319.3±4.8	71.6±5.2
		W8M	22		
6 Apr.	06:40	E2M	19	265.6±19.8	68.4±5.8
		W2L	30		
9 Apr.	22:18	E6U	4	84.3±13.8	46.4±5.8
		W6L	61		
24 Apr.	15:23	E2M	30	0.2±11.1	1.6±8.1
		W2L	5		
28 Apr.	21:28	E1U	11	123.7±18.7	55.9±6.4
		W1M	58		
1 Aug.	16:47	E6L	16	337.0±12.1	11.3±7.8
		W6M	13		
8 Aug.	16:36	E4M	20	136.1±15.5	36.1±8.0
		W4L	11		
14 Sept.	21:08	E6M	11	276.3±13.0	43.2±10.1
		W6M	13		
23 Sept.	05:40	E9L	18	240.5±8.7	3.1±7.3
		W9U	8		
26 Sept.	03:45	E3U	24	40.5±10.8	53.3±9.2
		W3U	20		
16 Nov.	18:06	E1M	14	278.3±14.1	24.8±10.4
		W1M	17		

TABLE III (Continued)

Date	G. M. T.	Elements	Energy deposition (MeV)	Right ascension (deg)	Declination (deg)
18 Jan. 1967	20:25	E2U W2U	14 20	22.3 ± 13.8	34.9 ± 10.4
23 Feb.	12:59	E9U W9M	20 25	267.0 ± 11.8	9.0 ± 8.2
7 Apr.	07:29	E8M W8M	19 21	52.9 ± 10.9	23.7 ± 5.6
9 May	22:08	E6L W6L	9 31	327.1 ± 9.8	42.3 ± 2.9
25 June	09:03	E3L W3L	22 24	28.4 ± 10.8	53.3 ± 9.2
2 July	04:56	E5L W5M	18 18	133.3 ± 12.2	4.2 ± 8.5
2 July	10:55	E7U W7U	37 234	31.7 ± 13.7	19.3 ± 10.1
13 July	17:31	E2M W2U	16 20	164.1 ± 11.9	13.3 ± 9.7
28 June 1965	21:39	E2U W2U W2M	60 8 5		
22 Aug.	02:33	E3L W3L W4L	130 ~100 ~100		
11 Nov.	22:28	E2 or 3M E3L W3U	~7 53 26		
18 Jan. 1967	16:25	E4U W4U W4M	163 80 8		

coincidence requirements. The majority of such seismic disturbances were directly attributable to blasting associated with the operation of the mine, and as such had a well-known temporal pattern. Others, however, were the result of the relaxation of strain in the unexcavated rock and thus occurred randomly.

Seismically induced signals fell into three categories: The vast majority had a signature similar to that produced by a particle penetrating a single detector element. The cause of such signals was determined to be electrostatic in origin. A frictional contact between the Lucite walls of a detector element and its light-tight Masonite housing was made and broken during the disturbance. It is conjectured that this produced a spark visible to the photomultipliers. The metal housings used in the second generation detector elements were considerably more rigid, and with rare exception, were not subject to this difficulty.

The second type of seismic trigger was of a microphonic nature, and had its origins in the amplifier electronics associated with the photomultipliers. Such signals were usually repetitive and, because of the manner in which groups of amplifiers were biased by common power supplies, could produce signatures similar to those associated with shower phenomena (category 2B).

A third type of seismic signal which also appears microphonic in nature was observed, but only rarely. These signals were uncoded collections of high- and low-frequency noise.

It is concluded that seismic disturbances of the first kind could not simulate neutrino signatures, although they could simulate single-tank events. The processes giving rise to electrostatic sparking are mechanical in nature and thus are not likely to occur within the system resolving time ($\sim 0.2 \mu\text{sec}$). Microphonic processes arising from seismicity could also not produce a neutrino signature

because two separately biased groups of amplifiers were involved in any neutrino-like event.

Because of the need to identify unambiguously the cosmic-ray component of the signal, seismic detectors were incorporated into the system early in its history, and only those events which were recorded in anticoincidence with seismic disturbances were used. Appropriate deadtime corrections were made.

V. THE DATA: SEPARATION OF ATMOSPHERIC AND NEUTRINO-INDUCED MUONS

Based on the detector geometry, the experimental data may be conveniently divided into a number of categories, as defined and detailed in Table II.

We interpret the data in terms of two distinct initiating sources: The more or less isotropic flux of muons produced by neutrinos interacting in the rock surrounding the detector and the sharply peaked vertical flux of atmospheric muons which penetrated the earth to our depth.¹⁶ Since our purpose here is to determine the flux of muons due to neutrinos, we must separate these two components. This was accomplished in two ways.

A maximum-likelihood calculation¹⁵ incorporating analytic forms for the two angular distributions was done to satisfy simultaneously the observed rate in each of the geometrically distinguishable classes of data.

A semiquantitative argument based on the two widely different angular distributions demonstrated that the events in category 1A (Table II) were due exclusively to neutrino-induced muons. The argument also allowed most of the category 1B events to be identified as in-aperture neutrino muons.

The maximum-likelihood method was developed for the calculation of the vertical atmospheric

muon contribution to the observed events. Its application to the calculation of the neutrino-induced component is somewhat limited by the implicit assumption of single-particle events. Multiple-particle events are considered in the more detailed argument. The two methods are discussed in Secs. VI and VII.

VI. MAXIMUM-LIKELIHOOD CALCULATION

For a combination of expected count rates, C_i , each one of which obeys a Poisson distribution, the likelihood function L may be written

$$L = \prod_{i=1}^{14} \frac{C_i^{N_i}}{N_i!} e^{-C_i}, \quad (1)$$

where N_i is the number of events observed¹⁷ in class i ,

$$C_i = t_i \int_0^\pi I(h, \theta) \frac{dA_i}{d\theta} d\theta, \quad (2)$$

where t_i is the sensitive time, $dA_i/d\theta$ is the differential aperture,¹⁵ and $I(h, \theta)$ is the sum of the atmospheric and neutrino-induced muon intensities. $I(h, \theta)$ can be written

$$I(h, \theta) = a_\mu j_\mu(h, \theta) + a_\nu j_\nu(\theta), \quad (3)$$

where θ is the zenith angle, h is the depth below surface, $j_\mu(h, \theta)$ and $j_\nu(\theta)$ are the angular distributions, and a_μ and a_ν are parameters which we fit to the data of our experiment by maximizing L . The subscript μ refers to atmospheric muons and ν to neutrino-induced muons. Limiting analytic forms were assumed for both the atmospheric and neutrino-muon angular distributions. As discussed in detail in Ref. 15, the limiting atmospheric muon angular distributions are given by

TABLE IV. Maximum-likelihood parameters. These numbers result from the data set chosen by Meyer *et al.* (Ref. 15). The somewhat different set of data chosen in this paper would change these numbers by about 2%. Since this is well within the errors quoted above, the data were not reevaluated. a_ν is the horizontal neutrino-induced muon flux. $a_\mu e^{-h/\lambda}$ is the vertical intensity of atmospheric muons at depth $h = 8.74 \times 10^5 \text{ g cm}^{-2}$.

Neutrino-induced muon angular distribution	Case Atmospheric muon angular distribution	Derived parameters		
		λ (10^4 g cm^{-2})	a_μ ($10^{-6} \text{ cm}^{-2} \text{ sec}^{-1} \text{ sr}^{-1}$)	a_ν ($10^{-13} \text{ cm}^{-2} \text{ sec}^{-1} \text{ sr}^{-1}$)
$1 - 0.67 \cos^2 \theta$ (horizontal to vertical ratio = 3)	$\sec \theta$	8.04	(1.11 ± 0.12)	(3.52 ± 0.66)
$1 - 0.67 \cos^2 \theta$ (horizontal to vertical ratio = 3)	Isotropic	8.08	(1.15 ± 0.12)	(3.53 ± 0.66)
Isotropic	$\sec \theta$	7.93	(1.20 ± 0.16)	(3.30 ± 0.62)
Isotropic	Isotropic	7.96	(1.25 ± 0.15)	(3.30 ± 0.62)

$$j_{\mu}(h, \theta) = e^{-h/\lambda} \cos^n \theta, \quad (4)$$

with

$$n = h/\lambda \quad (5)$$

or

$$n = h/\lambda - 1, \quad (6)$$

where

$$h = 8.71 \times 10^5 \text{ g cm}^{-2},$$

$$\lambda = (8.04^{+0.35}_{-0.39}) \times 10^4 \text{ g cm}^{-2}.$$

Neutrino-muon angular distributions are considered in Refs. 7 and 15. Table IV gives the parameters for the atmospheric and neutrino muon fluxes derived from this procedure.¹⁸ Table V gives the maximum-likelihood values and the observed populations for the various data categories.¹⁷

VII. DETAILED ARGUMENTS TO SEPARATE COSMIC-RAY AND NEUTRINO-INDUCED MUONS

Our object in what follows is to show that one class of our data (all categories but 1A and 1B) is consistent with a flux of high-energy muons and their associated showers peaked, to the vertical. We then argue that a second class (category 1A) is not attributable to vertical showers but is consistent with an approximately isotropic flux of neutrino-induced muons and their associated showers. Category 1B appears to contain a mixture of

events from both sources.

It is recognized that the separation effected in this way may not be precise, and that in a few cases, judgment based on incomplete information was required. Nevertheless, the number of misclassified events will be small and well within the given error bars. The various arguments detailed below may not by themselves be definitive, but as a group they are quite convincing.

The interactions by which muons produce showers include pair production, knock-on processes, bremsstrahlung, and photonuclear collisions.¹⁹ The number of such interactions per meter of rock versus burst energy for various initial muon energies is shown in Fig. 4. We chose 300 GeV as a representative atmospheric muon energy at our depth.²⁰ Taking into account the above interactions and the range-energy relationship for the resulting electrons²¹ we arrive at Fig. 5, which shows the fraction of incident muons interacting to produce a burst of energy capable of just reaching our detector as a function of the burst energy. For the muon energy representative of neutrino interactions, we chose²⁰ 10 GeV (see also discussion of category 5 events). The appropriate curve for this energy is also plotted in Fig. 5.

Data are available on the lateral development of showers in various materials for various burst energies.²² The data on aluminum were chosen since aluminum closely resembles rock in critical energy and radiation length (~15%). From these

TABLE V. Comparison of the observed data with the calculated number of events in each class. The data in this table are revised and differ slightly from those of Meyer *et al.* (Ref. 15). Calculations were performed with parameters derived from the experiment, using $\sec \theta$ enhanced atmospheric muons and two neutrino-induced muon angular distributions. Note for example that class 1UU contains events from categories 1A and 1B in which the muon was horizontal, i.e., the U-U, M-M, or L-L events, class 3UL contains events from category 3 which involved upper or lower elements.

Bays	Class	Observed number of events	Calculated number of events from maximum likelihood					
			Isotropic neutrinos			Nonisotropic neutrinos [$j_{\nu}(\theta) = 1 - 0.67 \cos^2 \theta$]		
			Atmospheric muons	Neutrino-induced muons	Total	Atmospheric muons	Neutrino-induced muons	Total
1-6	1UU	15	0.0	12.4	12.4	0.0	12.4	12.4
	1UM	10	0.0	12.5	12.5	0.0	12.4	12.4
	1UL	3	0.1	3.0	3.1	0.2	3.0	3.2
	3UL	102	80.9	37.9	118.8	81.6	37.8	119.4
	3M	41	23.3	14.0	37.3	24.1	14.0	38.1
	4A	37	40.7	2.6	43.3	39.4	2.6	42.0
	4B	25	8.5	0.3	8.8	8.0	0.3	8.3
7-9	1UU	3	0.0	2.9	2.9	0.0	2.9	2.9
	1UM	3	0.0	3.1	3.1	0.0	3.1	3.1
	1UL	1	0.04	0.9	1.0	0.1	0.9	1.0
	3UL	48	32.0	16.0	48.0	32.3	15.9	48.2
	3M	21	11.1	7.1	18.2	11.4	7.0	18.4
	4A	14	13.6	0.9	14.5	13.2	0.9	14.0
	4B	5	3.2	0.1	3.3	3.0	0.1	3.1

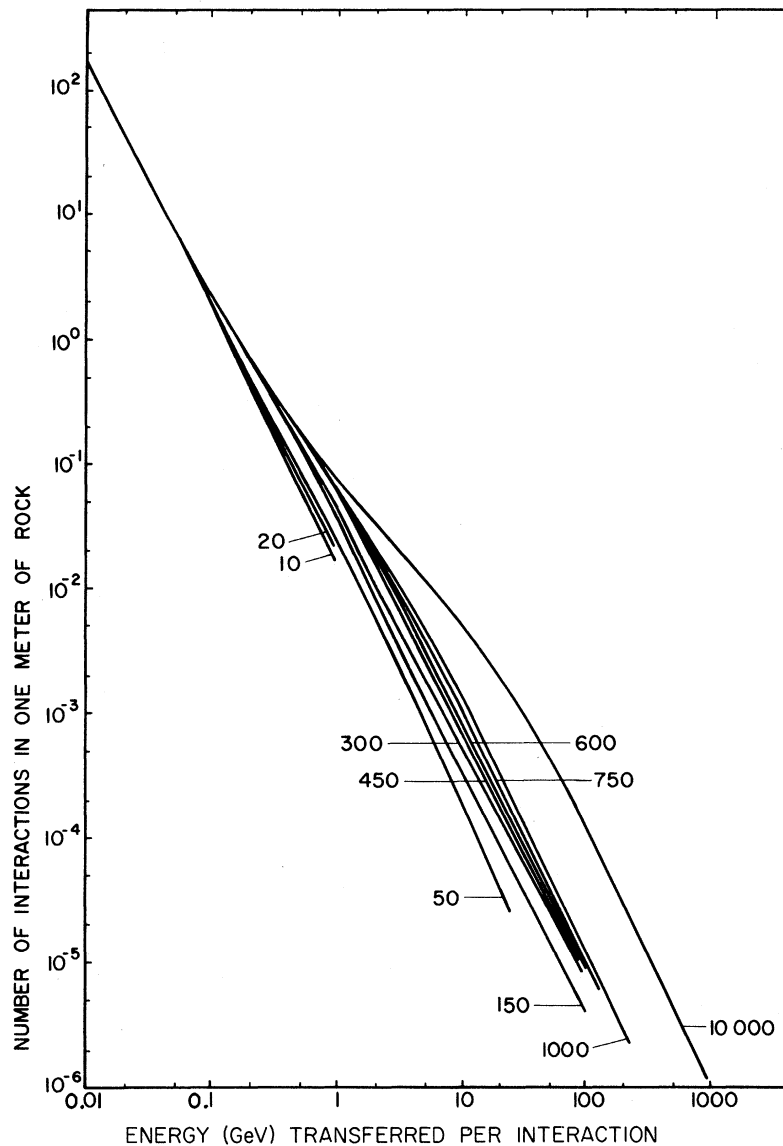


FIG. 4. Number of interactions in one meter of rock vs energy transferred to pair, γ -ray, or knock-on electron per interaction (for various initial muon energies).

results (see Fig. 6), it was clear that showers initiated by high-energy muons were capable of producing multitank cross-tunnel events such as those denoted by category 2A.

A. Arguments Which Indicate that Events Categorized as 1A Are Not Consistent with the Vertical Shower Picture but Are Consistent with Neutrino-Induced Muons

(a) Let us assume that *all* the observed events are due to atmospheric muons interacting in the rock surrounding the array. These interactions produce electromagnetic showers of various ener-

gies and widths which accompany the original muon. Based on the geometry of our array, we assign to each of our event categories a range of appropriate shower widths. Category 3, for example, would require a very narrow shower so that the event would indeed be confined to a single tank. Category 2A, on the other hand, requires a shower of a width which approximates that of the tunnel. Figure 7 is a plot of the fraction of total events versus the range of shower widths assigned to each category. In view of the strongly vertically peaked angular distribution of cosmic-ray muons, and the monotonically decreasing nature of the burst energy spectrum, Fig. 5, we expect a monotonically

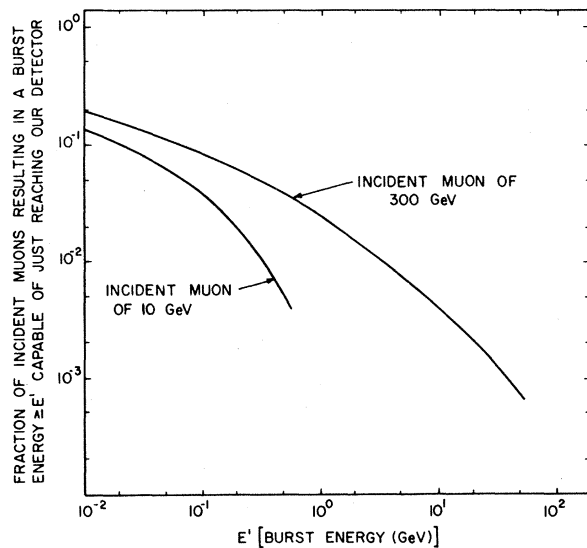


FIG. 5. The burst energy spectrum at our array for various incident muon energies.

decreasing fraction of total events with increasing shower width as defined above. This is, indeed, the distribution we observe when category 1A events are neglected. If, however, the category 1A events are included with the 1B and 2A data, we note a significant excess of events with large shower width.

(b) Another method of demonstrating this excess

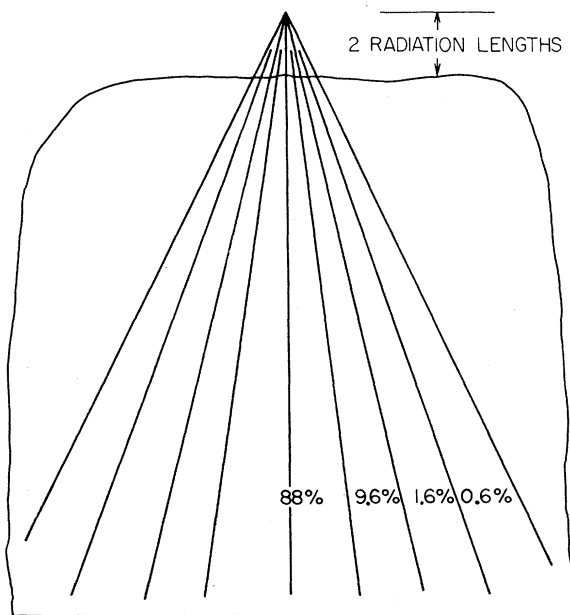


FIG. 6. The energy distribution in our tunnel due to a burst of 200 MeV occurring in the rock above the array.

of wide showers is to compare category 1A (two-tank cross-tunnel events) with categories 1B and 2A (cross-tunnel events involving more than two tanks). Here we assume that categories 1 and 2 are produced by cosmic-ray showers with a spread greater than or equal to the tunnel width. In order to produce such a large lateral development, it is necessary for many interactions to occur in the rock overburden. This implies many accompanying particles with a number distribution that decreases as one goes further from the shower center.²² As a consequence, it is highly unlikely for a shower to produce events in two tanks on the periphery of its development and at the same time, not produce events in tanks closer to the shower center. Accordingly, two-tank cross-tunnel events (1A) are less likely than cross-tunnel events involving more than two tanks (1B, 2A).²³ In our data, however, there are 31 1A events while the 1B and 2A categories total 14. Clearly, a mechanism other than large vertical showers must be responsible for 1A events. A consideration of the detector geometry reveals that this argument is incomplete, since for 1A events involving two bottom tanks, the central part of the shower could miss the other tanks. This point is discussed in the following paragraph.

(c) One can make another argument against the large vertical-shower origin of category 1A based on the event distribution within the 1A category itself. Within the admittedly poor statistics, the numbers of Upper-Upper (U-U), Middle-Middle (M-M), and Lower-Lower (L-L) events are equal (the numbers are U-U=5, M-M=4, and L-L=6). As in paragraph (b) above, this would not be expected if the 1A events were due to showers from above.

(d) A possible source of category 1A events is an interaction producing a single particle which is

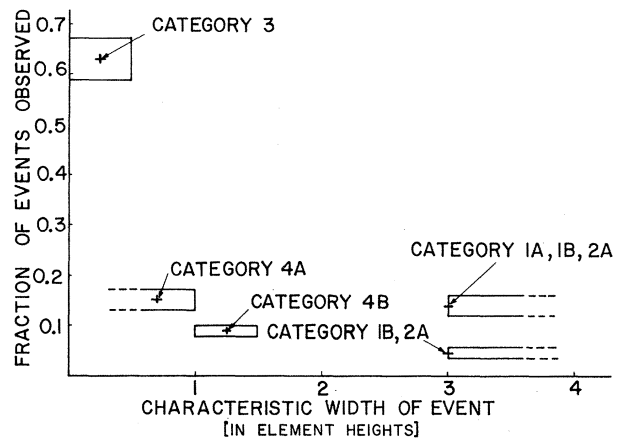


FIG. 7. Decoherence curve to infer separation of data between atmospheric and neutrino-induced muons.

then scattered at a large angle from the incident muon. Since the angular distribution of the scattered single particle is peaked in the direction of the incident muon, one would expect a much larger number of U-L type 1A events than U-U events. This is contrary to the observed data: U-L=4 and U-U=5.

(e) If we examine the energy deposited by 1A events (Table III) in each detector element in terms of the geometrically expected deposition modified by the detector resolution function,²⁴ we find that 29 of the 32 events are consistent with single particles (Fig. 8). The remaining three events have large (>100 MeV) energy depositions in one of the two tanks. The large energy deposition is attributed to secondary particles accompanying the muon. In the three events in question, the apparent inclination from the zenith is so large as to rule out a cosmic-ray muon as the cause (Fig. 9). In one of these, however, we judge that the muon missed a detector and is, therefore, out

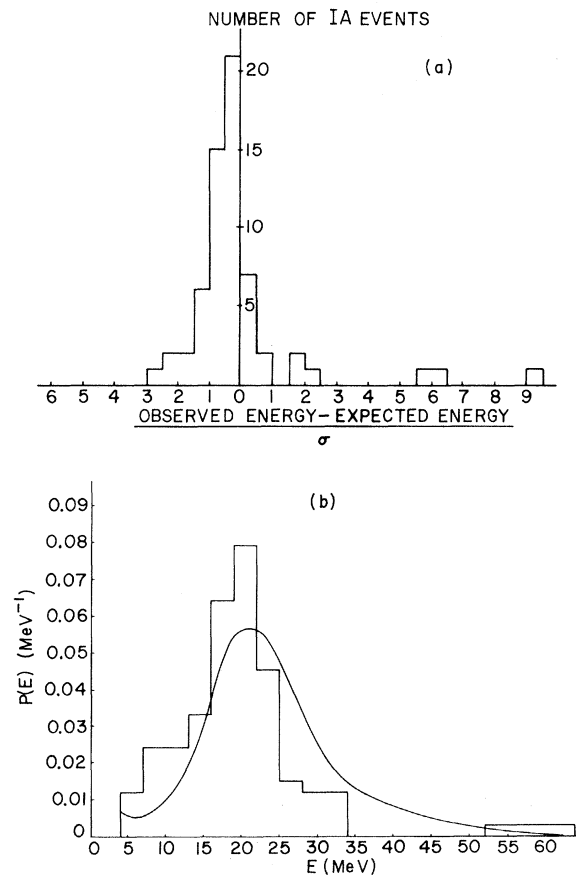


FIG. 8. (a) Deviation from expected energy deposition in 1A events. (b) The observed energy deposited in category 1A events compared to the expected spectrum. Effects of Landau broadening, corner clipping, and detector energy resolution have been included.

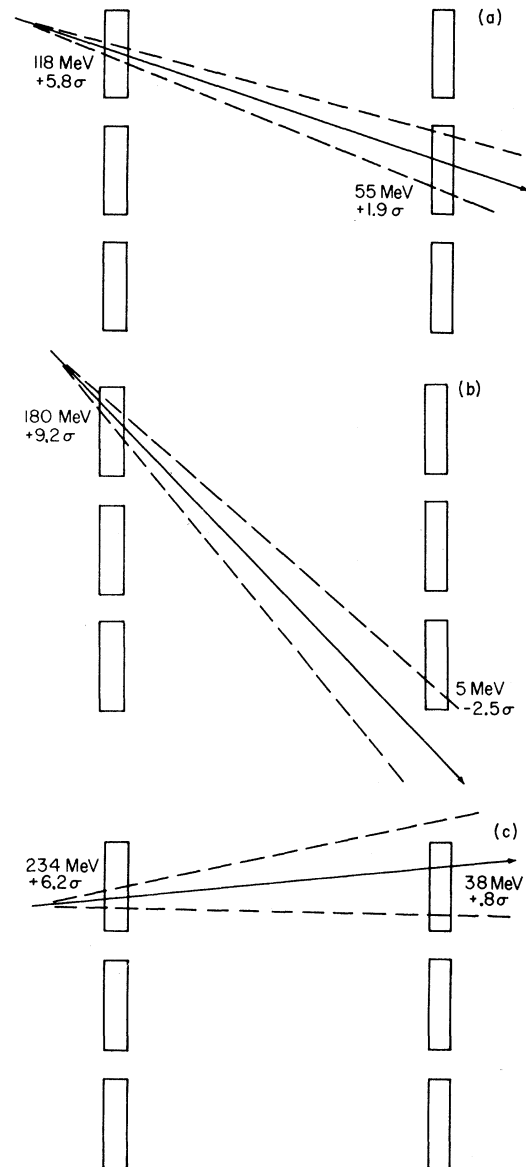


FIG. 9. Category 1A events which do not satisfy a single-particle interpretation: (a) Event of 28 February 1965. The energy depositions are consistent with a muon plus secondaries passing through both elements. The large zenith angle implies a neutrino-induced muon. The absence of signals from other elements precludes a vertical cosmic-ray shower. (b) Event of 8 October 1966. The energy depositions are consistent with a muon plus secondaries passing through the upper element, but the muon and most secondaries missing the lower element. Such an event is out of the geometry used to calculate the neutrino-induced muon flux. (c) Event of 2 July 1967. The energy depositions are consistent with a muon plus secondaries passing through both elements, although the evidence is not as strong as in the event of 28 February 1965. The large zenith angle implies a neutrino-induced muon. The absence of signals from other elements precludes a vertical cosmic-ray shower.

of the aperture used for calculation of fluxes. Consistent reconstructions of these three events are depicted in Fig. 9.

(f) Yet another component of the cosmic rays which could produce the 1A signature are multiple-muon showers. These consist of a bundle of nearly parallel muons produced in the interaction of a single cosmic ray primary and its progeny, and typically spread over an area of 100 to 300 m². Cannon and Stenerson²⁵ have recently measured the intensities for simultaneously detecting two and three muons in a large detector. According to these measurements, the probability of a single muon being accompanied by another is only about 1%. Since there were about 300 single muons which passed through our detector, we would expect about three of these to be paired. In order to simulate a neutrino event, the accompanying muon must also hit the detector, and further, must satisfy a rather rigorous set of geometrical requirements. These considerations reduce the number of 1A events produced by this mechanism to $\ll 1$ in our run time.

B. Some Arguments Indicating that Events Other Than Those Categorized as 1A and 1B are Consistent with Vertical-Shower Picture

(a) Using the vertical intensity at our site,¹⁵ we calculate that the total number of atmospheric muons which penetrated our tunnel in the immediate vicinity of the detector was ~ 1100 in the total run time. In this time, we observed 10 category 2A events. We conclude, therefore, that we observe cosmic-ray showers of large extent about 1% of the time. The average energy deposited in our detector by the category 2A events was greater than 600 MeV. The average burst energy must, therefore, have been considerably in excess of this. One would predict from Fig. 5 that 1% of the cosmic rays incident upon our detector array would have a shower of 4 GeV or greater accompanying them.

(b) We would expect more M-L events than U-M events in category 4A. This is because many potential single-particle U-M events become category 4B (i.e., U-M-L) events by virtue of their accompanying particles, and are lost to the category (see Fig. 10). In addition, muons which would miss our apparatus if unaccompanied by secondaries can, by virtue of these secondaries, produce more M-L events than U-M events. We observe 35 M-L events and 15 U-M events. This is consistent with our prediction.

A comparison of category 4A with 4B shows, as one would expect, that the calculated ratio of apertures¹⁵ for single-particle cosmic-ray events

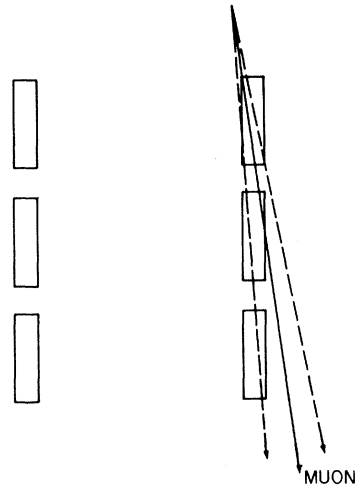


FIG. 10. A category 4A U-M becomes a category 4B by virtue of its accompanying secondaries.

(6.5/1.2) is very much greater than the observed ratio of events (51/30).

We note also that the 4B data can be examined in terms of the expected energy deposition for a single particle. Only a fraction of the events satisfy the expected range of single-particle energies. This fraction is consistent with the number of single-particle 4B events predicted based on our aperture.

(c) A comparison of the 1B and 2A data shows that those events involving greater than three elements are more probable than those involving only three. In addition to corroborating our shower picture, this argument further strengthens that given in Sec. VIIA, paragraph (b).

(d) Category 2A events are never observed to involve an Upper and Middle without a Lower. This, too, would be predicted by our shower picture.

C. Category 1B Events

If we examine the 1B events individually, we find that in most cases only one trajectory can be assigned consistently within the constraints of the two-component flux of muons discussed above.

For example, in the event of 18 January 1967 (Fig. 11), a horizontal track of the type illustrated with its accompanying shower seems the most likely reconstruction. It is, of course, conceivable that this event was produced by a vertical shower, but in our view, based on the arguments given in Secs. VIIA and VII B, this interpretation is highly improbable. Thus, we believe this event should be attributed to a neutrino interaction.

Proceeding in this fashion, we assign four of the 1B events to horizontal muon showers produced by

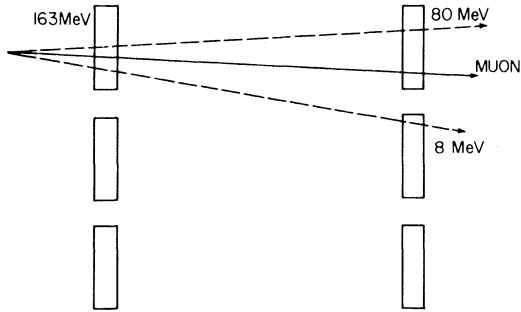


FIG. 11. Event of 18 January 1967. A category 1B event interpreted as a horizontal muon with accompanying shower.

neutrinos, and one to a vertical cosmic-ray shower. This leaves one event lacking a unique interpretation, but we judge this to be most likely attributable to a cosmic-ray muon.

D. Category 2A Events

The arguments in Sec. VII C suggest that a portion of the category 2A events may be due to horizontal showers, i.e., neutrino-induced muons with associated particles. One can see, however, that the number of such events from vertical showers (atmospheric muons plus a smaller component from neutrino muons) must greatly exceed that from horizontal showers. This follows both from the relative probabilities with which atmospheric and neutrino muons make showers of a given energy (Fig. 5), typically $\geq 2/1$, and from the large ratio of vertical to horizontal muons (~ 213 to 35). As a result, $< \frac{1}{2} \times \frac{35}{213} \times 8 < 1$ category 2A events can be attributed to "horizontal" neutrino-induced showers.

E. Multiple-Particle Neutrino Events

From Fig. 5, we would expect about 86% of our "in-aperture" neutrino events to have showers of 10 MeV or less accompanying the muon, i.e., to be consistent with unaccompanied muons. We see 35 total in-aperture neutrino events and, there-

fore, predict that 30 of these should be consistent with a single particle. We observe 29, a result in agreement with our prediction.

F. Category 5 Events - Delayed Coincidences

During the course of the experiment, four events classified as category 5 were recorded. These are characterized by a pattern of chronotron pulses which do not conform to the expected patterns for horizontal and vertical single particles or bursts. However, the pattern of pulses for these four events can be recognized with good certainty as being caused by two particles which deposit energy in a single element at approximately the same location a few microseconds apart. Table VI gives results of analysis of these events. The observed mean time interval of $3.2 \mu\text{sec}$ is sufficiently close to the $2.2 \mu\text{sec}$ characteristic of muon decay that it seems highly probable that the prompt signal represents a stopping muon and the delayed signal its decay electron. Table VI also shows that the energy deposited by the first particle is large, as expected for a muon nearing the end of its range, and that the energy deposited by the delayed particle in most cases is consistent with the muon β -decay spectrum (53 MeV end-point energy). The too-high decay energy for the first event may possibly be accounted for by the fact that this energy is a somewhat rough estimate based on the slope of a pulse whose amplitude is in the saturated region.

Assuming that these events are indeed muon decays, the question arises whether they are decays of atmospheric or neutrino-produced muons. (Since the experiment features a unique site and an array of detectors unlike any used previously, we should allow the possibility of some hitherto undetected source of low-energy muons.) The possibility that they are decays of atmospheric muons can be ruled out by the following argument: Since the vertical intensity of cosmic-ray muons can be represented by¹⁵

$$I_V(h) = a_\mu e^{-h/\lambda}, \quad (7)$$

TABLE VI. Muon decay data.

Date	G. M. T.	Element	Energy deposition (MeV)		Location (meters from north end of element)		Time delay (μsec)
			E prompt	E delayed	Prompt	Delayed	
19 Apr. 1965	23:33	EIL	147	97	2.1	1.8	4.2
16 Jan. 1966	04:12	WIU	22	12	0.1	0.1	2.2
31 May 1966	18:36	WIL	38	20	0.83	0.38	3.4
23 May 1967	05:40	W4M	152	16.4	2.58	2.88	2.85
							3.2 (mean)

the fractional decrease in the vertical intensity with depth is given by

$$\frac{1}{I_V} \frac{dI_V}{dh} = -\frac{1}{\lambda}. \quad (8)$$

The mean thickness of the detector array for traversing atmospheric muons is estimated from the observed mean energy deposition to be $\sim 30 \text{ g cm}^{-2}$, while λ at our site has the value¹⁵ $8.04 \times 10^{-4} \text{ g cm}^{-2}$. Therefore, we expect that only about 0.04% of these muons will stop. It is seen from Table V that ~ 213 atmospheric muons were detected, thus the predicted number which will stop is ~ 0.1 . The four events which occurred must, therefore, be caused by a flux of muons of significantly lower energy, which we now estimate.

An estimate is first made of the probable number of muons which stopped in the array, some of which may not have given identifiable category 5 signals. Corrections must be made for the following:

(1) the finite oscilloscope display time for each event, which allows $\sim 20\%$ of the decay electrons to escape observation;

(2) the $\sim 10 \text{ MeV}$ minimum energy required to give an observable decay electron signal. About 30% of the decay electrons do not deposit sufficient energy in the element to give detectable chronotron pulses;

(3) loss of muons by nuclear capture. For our scintillator liquid (CH_2), about 2% of the total muon flux will be lost by this process.

Making these corrections, we believe that the number of potential category 5 events was 7 ± 4 .

The probability that a neutrino-induced muon with range R in rock will stop in an element of effective thickness d is d/R . For these muons $d \sim 20 \text{ g cm}^{-2}$. Since the total number of neutrino-induced muons penetrating our detector was ~ 113 (see Table V), the number of stopping muons is $113d/R$. From this, the average range of the muons which stop is $\sim 300 \text{ g cm}^{-2}$, suggesting a most probable muon energy of about $\frac{1}{2} \text{ GeV}$.

Wolfendale *et al.*²⁶ have estimated the low-energy part of the neutrino spectrum, and from it the fraction of low-energy muons stopping in our detector. Their result, about 4%, implies that ~ 4.5 neutrino-induced muons stopped. This agrees with the observed number and our own estimate, and may be regarded as further evidence of our observation of neutrino-induced muons. We therefore conclude that the type 5 events are due to muon decay and are compatible with the decay of neutrino-induced muons.

G. Accuracy of the Data Separation

The above arguments demonstrate that cosmic-ray neutrinos have been observed. We now address ourselves to the accuracy with which the separation of cosmic-ray and neutrino-induced muons has been accomplished. Despite the compelling arguments given above, we recognize the possibility that a small number of events may have been incorrectly attributed to neutrinos. As an *upper limit* on this number, we assume that *all* multiparticle events classified as neutrinos (two category 1A events and four category 1B events) were, in fact, misclassified. This is a conservative assumption since the number of multiparticle neutrino events is consistent with expectations (Sec. VII A, paragraph (e)). Even with this extreme assumption, the overestimate in the neutrino signal ($\sim 17\%$) is no larger than the error we quote for our neutrino-induced muon rate.

It is important to note that the physical conclusions based on our experiment⁷ become more powerful as the signal rate is lowered.

VII. CORRECTIONS TO THE DATA

(a) As noted, the spatial variation in detector response meant that an event at a given energy deposition had a detection efficiency which depended upon location as well as discrimination level. A determination of this efficiency was made possible by using the energy spectrum of the 1A events as a first approximation to the actual probability of various energy depositions. Since an energy deposition in excess of the discriminator level was necessary only in one of the two elements involved in a 1A event, this approximation is expected to be quite good. This probability was then integrated over the location-dependent efficiency for providing a trigger pulse, thus determining the detector efficiency for the system to be 97% for the first six bays and 100% for the remaining three bays.

(b) Systematic light-pulsar (Sec. II) event simulation revealed those parts of the array which were on occasion unable to trigger the system. Corrections were made to the run times of the affected categories; e.g., if one photomultiplier tube became faulty, then its element was insensitive to single-element events, but still sensitive to multi-element events in which one of the other elements could trigger the system. Such dead times were estimated by counting from the last test which showed the element to be active.

IX. NEUTRINO-INDUCED MUON FLUX

Application to the data of the corrections and

selection processes outlined above, leads to a measured rate of $(6.5 \pm 1.1) \times 10^{-7} \text{ sec}^{-1}$ for observing neutrino-induced muons. The determination of a total neutrino-muon flux from these rates is complicated by the energy dependence of both the flux and angular distribution of the muons. A theoretical calculation of the rates involves an integration of the differential aperture of the detector¹⁵ and the energy-dependent angular distribution over zenith angle followed by an integration, over the muon spectrum. A knowledge of this spectrum requires information on the neutrino interaction cross sections which is not available experimentally for energies in excess of 10 GeV. Such calculations are made for various assumed forms for the neutrino cross section in a companion paper,⁷ and the results compared with the experimental rate.

To facilitate comparison with the results of our maximum-likelihood calculation and with the results of others, we here calculate the flux assuming the neutrino-induced muons to be isotropic. On this assumption, the muon flux is found to be $(3.7 \pm 0.6) \times 10^{-13} \text{ cm}^{-2} \text{ sec}^{-1} \text{ sr}^{-1}$. It can be seen from Table IV that the two methods of calculation are in good agreement. The existing discrepancy can be attributed to the different classes of data employed by the two calculations. The maximum-likelihood calculation is based on all data classes listed in Table V, while the second approach uses only those events which we attribute to neutrino-induced muons (Table III).

X. OTHER EXPERIMENTAL RESULTS

A. An Improved ERPM Experiment

The work described in this paper was performed primarily as a first foray into the field. It was recognized at the outset that the spatial ($\pm 15 \text{ cm}$ longitudinal and $\pm 30 \text{ cm}$ vertical) and angular resolution ($\pm 10^\circ$) was at best rudimentary, and the anticipated (and actual) event rate was quite low. A much more sophisticated and enlarged detector using a large number ($\sim 50\,000$) of flash tubes and scintillation triggers has been developed by this group and should yield results which have a spatial resolution of a few centimeters, an angular resolution of a few degrees, and double the neutrino signal rate.

Preliminary results of this improved experiment²⁷ give a neutrino-induced muon flux of $(3.9 \pm 0.7) \times 10^{-13} \text{ cm}^{-2} \text{ sec}^{-1} \text{ sr}^{-1}$ for an assumed isotropic muon distribution.

B. Kolar Gold Fields Experiment

An experiment performed in the Kolar Gold Fields²⁸ at a vertical depth of $7.6 \times 10^5 \text{ g cm}^{-2}$ of

standard rock gave a neutrino-induced muon flux of $(2.6 \pm 0.7) \times 10^{-13} \text{ cm}^{-2} \text{ sec}^{-1} \text{ sr}^{-1}$ for an assumed isotropic angular distribution.

The rough agreement between the three experiments is additional evidence for the neutrino origin of the signals in each, particularly when one considers that the atmospheric muon background at the ERPM sites was about an order of magnitude below that of the Kolar experiment.

ACKNOWLEDGMENTS

Dr. T. L. Jenkins and B. M. Shoffner were most helpful in the early stages of this work. R. Atkinson and J. Baird helped in the maintenance and operation of the equipment. G. Nelson and M. Stein read and assisted in interpreting film records. We gratefully note the assistance and cooperative attitude of the men of the East Rand Proprietary Mines. A special word of appreciation is due our engineer, A. A. Hruschka, for his vital part in the design, construction, and installation of the detector and laboratory deep underground.

APPENDIX: THE CHRONOTRON

The basic element in the chronotron system was the "chronotron box," accommodating (as shown in Fig. 12) 24 input signals, arranged as a 4×6 matrix. Each input signal produces three outputs, two indicating the row and column address of the signal, and the third identifying the box itself. The output signals were unity-gain replicas of the input.

Six such boxes were cabled together by means of

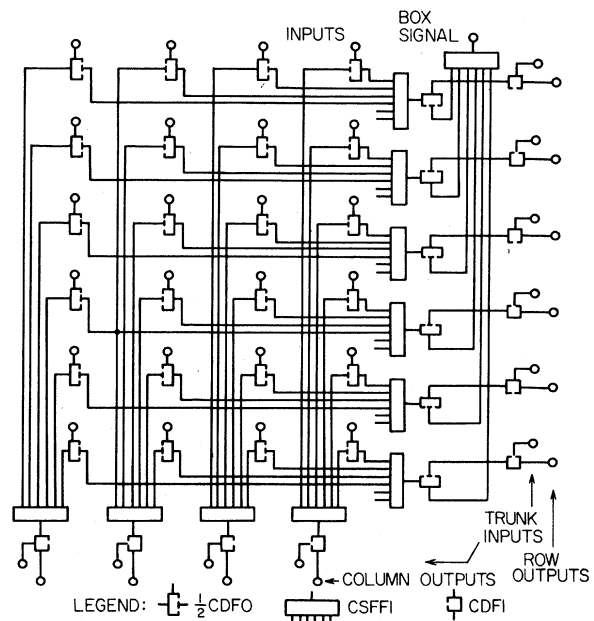


FIG. 12. A chronotron box (4×6 matrix).

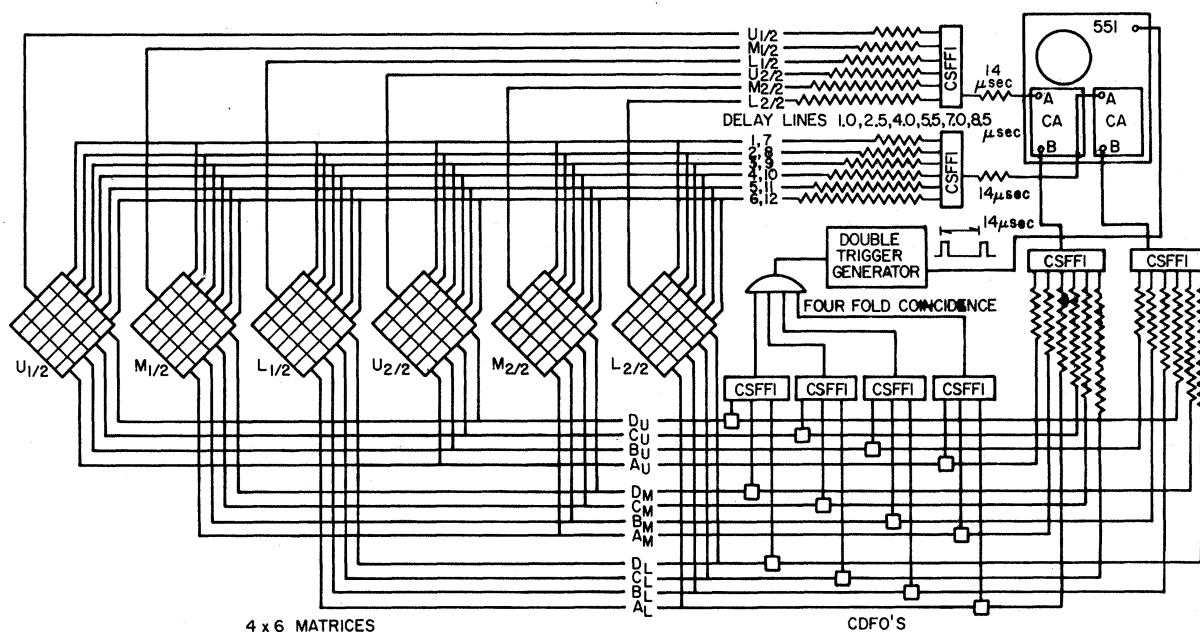


FIG. 13. Block diagram of chronotron system for one side of the detector hodoscope.

a trunk line for each column and each row (Fig. 13). This produced a single matrix capable of handling 144 inputs and having 24 outputs. The hodoscope was divided into two rails (east and west). Correspondingly, two of the units just described were employed.

The box circuitry consisted of a number of fan-outs and fan-ins and a matrix of signal cables. The design of these circuits and cables and the power supply system required considerable care to minimize cross talk so that a given input signal did not give rise to output signals in other rows or columns.

In its final form, Upper, Middle, and Lower signals were connected to separate boxes (six bays per box). Thus, the box pulse identified the detector element as Upper, Middle, or Lower. Within each box the A, B, C, and D photomultiplier signals were associated with the four rows, while each bay was assigned its own column. Thus, the column signal identified the bay while the row signals presented the individual signal amplitudes and waveforms.

The block diagram (Fig. 13) shows the interconnection of the chronotron boxes, delay lines, and the recording oscilloscope along with a simplified version of the necessary logic circuitry. Two such circuits existed, one for the east rail and one for the west rail.

Also shown in Fig. 13 is the discriminator and coincidence circuitry. The fan-out (CDFO) and fan-in (CSFFI) circuits served to combine appropriate groups of signals, e.g., signals from all A

tubes (Upper, Middle, and Lower). These were in turn fed into a discriminator circuit (Schmitt triggers) and a pulse shaping circuit (single-shots). The four sets of signals (all A's, all B's, all C's and all D's) which were then logic levels, were fed into a fourfold coincidence circuit (nand gate). The resolving time of the trigger logic was determined by the width of the single-shot pulse to be $\sim 0.8 \mu \text{ sec}$. Thus, the coincidence requirements for the array were, any A, and any B, and any C, and any D. In fact, four complete and independent discriminator-coincidence circuits were employed. These served the east and the west sides of the bays 1-6 and the east and west sides of 7-9.

The capacity of the dual-beam oscilloscope for display of signals was increased by sweeping twice to give a four-trace raster. This required that the locator signals be stored in delay lines for an additional period slightly greater than the $13\text{-}\mu \text{ sec}$ sweep duration.

The logic circuits used to trigger the recording oscilloscope and the Beattie-Coleman scope camera are composed principally of nand gates, nor gates, diode clusters, and single-shot multivibrators in the form of 0.5-MHz commercial logic cards. The circuits are somewhat more complex than indicated on the schematic because of various block circuits, camera control circuitry, geophone coincidence circuitry, etc.

Reference is made to an article by Crouch *et al.*²⁹ for a more extensive discussion of the chronotron system.

*Supported in part by the U. S. Atomic Energy Commission.

†Now at the Weizmann Institute, Rehovoth, Israel.

¹K. Greisen, in *Proceedings of the International Conference on Instrumentation in High-Energy Physics, Berkeley, California, September, 1960* (Interscience, New York, 1961), p. 109.

²M. A. Markov, in *Proceedings of the Tenth Annual International Rochester Conference on High-Energy Physics, 1960*, edited by E. C. G. Sudarshan, J. H. Tinlot, and A. C. Melissinos (Interscience, New York 1960), p. 385.

³M. A. Markov and I. M. Zeleznykh, *Nucl. Phys.* 27, 385 (1961).

⁴G. Danby, J. M. Gaillard, K. Goulianos, L. M. Lederman, N. Mistry, and J. Steinberger, *Phys. Rev. Letters* 9, 36 (1962).

⁵S. Miyake, private communication; S. Miyake, V. S. Narasimham, and P. V. Ramana Murthy, in *Proceedings of the International Conference on Cosmic Rays and the Earth Storm, Kyoto, Japan, September, 1961*, Vol. III, p. 318 [Suppl. J. Phys. Soc. Japan 17, 318 (1961)].

⁶Brief reports of the findings with the first bays of this facility were published in 1965: F. Reines, M. F. Crouch, T. L. Jenkins, W. R. Kropp, H. Gurr, J. P. F. Sellschop, and B. Meyer, Informal Conference on Experimental Neutrino Physics, CERN, 1965 (unpublished), and F. Reines, M. F. Crouch, T. L. Jenkins, W. R. Kropp, H. S. Gurr, G. R. Smith, J. P. F. Sellschop, and B. Meyer, *Phys. Rev. Letters* 15, 551 (1965).

⁷H. H. Chen, W. R. Kropp, H. W. Sobel, and F. Reines, following paper, *Phys. Rev. D* 4, 99 (1971).

⁸This is the actual depth. It is customary to quote depth in standard rock in order to facilitate the comparison between the various experimental locations. Our depth in standard rock is 8.74×10^5 g cm⁻². Geological data relevant to the experiment are discussed briefly in Ref. 14. A more extensive treatment is contained in an internal report, H. W. Sobel and W. R. Kropp, University of California, Irvine, Report No. UCI-10P19-44 (unpublished).

⁹H. Faissner, F. Ferrero, A. Ghani, and M. Reinharz, *Nucl. Instr. Methods* 20, 289 (1963). See also J. Barton *et al.*, *J. Sci. Instr.* 39, 360 (1962); 41, 736 (1964).

¹⁰When filled with the highly transparent and stable mineral-oil-based scintillator [T. L. Jenkins and F. Reines, *IEEE Trans. Nucl. Sci. NS-11*, 1 (1964)], the detector element length was found to be limited in our case by the logistics of transport to the underground site.

¹¹M. F. Crouch, H. S. Gurr, A. A. Hruschka, T. L. Jenkins, W. R. Kropp, F. Reines, and H. W. Sobel, *IEEE Trans. Nucl. Sci. NS-13*, 424 (1966).

¹²Sidereal coordinates of the events in category 1A are given in Table III. Limits on extraterrestrial neutrinos are discussed in Ref. 7.

¹³B. M. Shoffner and T. L. Jenkins, *IEEE Trans. Nucl. Sci. NS-13*, 438 (1966).

¹⁴H. S. Gurr, Ph.D. thesis, Case Institute of Technology

(now Case Western Reserve University), 1966 (unpublished).

¹⁵A previous paper [B. S. Meyer, J. P. F. Sellschop, M. F. Crouch, W. R. Kropp, H. W. Sobel, H. S. Gurr, J. Lathrop, and F. Reines, *Phys. Rev. D* 1, 2229 (1970)], which focuses on the determination of the cosmic-ray muon depth-intensity curve, contains some of the material presented in the present paper. This overlap is considered desirable for clarity and completeness.

¹⁶Both the atmospheric muons and the neutrinos arise primarily from *K* and π decay. Deep underground the angular distribution of atmospheric muons is sharply peaked to the vertical because of the steeply falling spectrum coupled with the increased absorption associated with departures from the vertical. On the other hand, the atmospheric neutrinos are not significantly attenuated by the earth and, hence, retain their initial, angular distribution which favors the horizontal direction.

¹⁷The data for each half of the array was further sorted into seven classes, where each class represented a particular range of zenith angles. Table V lists all 14 classes.

¹⁸As discussed in Ref. 15, the angular dependence of the cosmic-ray muons is a function of a_μ and λ necessitating an iterative process involving the depth intensity curve.

¹⁹I. L. Rosental, *Usp. Fiz. Nauk* 94, 91 (1968) [*Soviet Phys. Usp.* 11, 49 (1968)].

²⁰R. Craig, J. L. Osborne, A. W. Wolfendale, and E. C. M. Young, *Proc. Phys. Soc. (London)* 1, 61 (1962).

²¹M. J. Berger and S. M. Seltzer, National Academy of Sciences—National Research Council Report No. 1133 (1966).

²²A. Kantz and R. Hofstadter, *Nucleonics* 12, No. 3, 36 (March, 1954).

²³This conclusion runs counter to the superficially attractive argument that it is easier to produce "simpler" (i.e., 1A) events than the more complicated multitank events.

²⁴B. S. Meyer, Ph.D. thesis, University of the Witwatersrand, 1969 (unpublished).

²⁵T. M. Cannon and R. O. Stenerson, *J. Phys. A* 4, 266 (1971).

²⁶A. W. Wolfendale and E. C. M. Young, in *Proceedings of the Neutrino Meeting, CERN, 1969* (CERN, Geneva, 1969).

²⁷W. G. Sandie, P. B. Landecker, D. Bourne, M. F. Crouch, J. Lathrop, J. P. F. Sellschop, H. W. Sobel, and F. Reines, in *Proceedings of the Sixth Interamerican Seminar on Cosmic Rays, LaPaz, Bolivia, 19-24 July 1970* (Laboratorio de Física Cosmica, Universidad Mayor de San Andrés, LaPaz, Bolivia, 1970), Vol. 4, p. 833.

²⁸M. R. Krishnaswamy, M. G. K. Menon, V. S. Narasimham, K. Hinotani, N. Ito, S. Miyake, J. L. Osborne, A. J. Parsons, and A. W. Wolfendale, *Proc. Roy. Soc. (London)* (to be published).

²⁹M. F. Crouch, H. S. Gurr, W. R. Kropp, B. Meyer, and F. Reines, *IEEE Trans. Nucl. Sci. NS-13*, 432 (1966).